The Journal of Experimental Biology 208, 3519-3532
Published by The Company of Biologists 2005
doi:10.1242/jeb.01813

On the estimation of swimming and flying forces from wake measurements

John O. Dabiri

Graduate Aeronautical Laboratories and Bioengineering, California Institute of Technology, Pasadena, CA 91125, USA

e-mail: jodabiri@caltech.edu

Accepted 19 July 2005

Summary

The transfer of momentum from an animal to fluid in its wake is fundamental to many swimming and flying modes of locomotion. Hence, properties of the wake are commonly studied in experiments to infer the magnitude and direction of locomotive forces. The determination of which wake properties are necessary and sufficient to empirically deduce swimming and flying forces is currently made *ad hoc*. This paper systematically addresses the question of the minimum number of wake properties whose combination is sufficient to determine swimming and flying forces from wake measurements. In particular, it is confirmed that the spatial velocity distribution (i.e. the velocity field) in the wake is by itself insufficient to determine swimming and flying forces, and must be combined with the fluid pressure distribution. Importantly, it is also shown that the spatial distribution of rotation and shear (i.e. the vorticity field) in the wake is by itself insufficient to determine swimming and flying forces, and must be combined with a parameter that is analogous to the fluid pressure. The measurement of this parameter in the wake is shown to be identical to a calculation of the added-mass contribution from fluid surrounding vortices in the wake, and proceeds identically to a measurement of the added-mass traditionally associated with fluid surrounding solid bodies. It is demonstrated that the velocity/pressure perspective is equivalent to the vorticity/vortex-added-mass approach in the equations of motion. A model is developed to approximate the contribution of wake vortex added-mass to locomotive forces, given a combination of velocity and vorticity field measurements in the wake. A dimensionless parameter, the wake vortex ratio (denoted Wa), is introduced to predict the types of wake flows for which the contribution of forces due to wake vortex added-mass will become non-negligible. Previous wake analyses are re-examined in light of this parameter to infer the existence and importance of wake vortex added-mass in those cases. In the process, it is demonstrated that the commonly used time-averaged force estimates based on wake measurements are not sufficient to prove that an animal is generating the locomotive forces necessary to sustain flight or maintain neutral buoyancy.

Key words: swimming, flying, locomotion, vortex, force, wake.

Introduction

The vortex wake is the fluid dynamic footprint of swimming and flying animals. When an animal moves through fluid, Newton's second and third laws together dictate that the locomotive force exerted by the fluid on the animal has a magnitude equal to the rate at which the animal imparts momentum to the fluid. Often the animal delivers this momentum in the form of rotating fluid masses called vortices. Since the vortex wake created by an animal during locomotion persists for some time after the forces needed to initiate locomotion have been achieved, the vortex wake serves as a temporary record of the animal–fluid interactions from which locomotion arises.

A self-propelled animal moving at constant velocity experiences no net force and therefore delivers no net momentum to the wake *via* these fluid vortices. However, any time the animal accelerates, fluid momentum exists in the vortex wake that can be probed to deduce the locomotive forces generated by the animal. Despite the common approximation of 'steady locomotion', in which it is assumed that the animal does not accelerate from its nominal cruising speed, nearly all swimming and flying animals continually exhibit linear and angular accelerations during locomotion, both parallel and perpendicular to the direction of travel, which are related to starting, stopping, maneuvering and cruising. Hence, measurements of the vortex wake can elucidate physical principles governing nearly every aspect of swimming and flying locomotion.

An exact determination of swimming and flying forces based on measurements of the surrounding fluid requires precise knowledge of both the flow in the wake of the animal and the flow near its body. Noca et al. (1997, 1999) derived the complete set of equations necessary to measure instantaneous, unsteady (time-dependent), forces on a body based on the velocity of flow around the body and in the wake.

Due to practical difficulties in experimentally measuring the flow close to the body of an animal, recent efforts have focused on estimating the forces generated by swimming and flying animals based on properties of vortex wake alone. Of the various properties that one can measure in a vortex wake, those that are most commonly examined in the literature are the velocity, vorticity (rotation and shear), and pressure.

Pressure measurements are generally difficult to accomplish and have rarely been achieved in studies of swimming and flying animals (for an exception, see Usherwood et al., 2005). Velocity and vorticity are more easily measured in the wake due to advent of quantitative measurement techniques such as digital particle image velocimetry (DPIV; cf. Drucker and Lauder, 1999; Spedding et al., 2003; Warrick et al., 2005). These velocity and vorticity measurements are typically presented in an Eulerian frame, for which the velocity and vorticity are defined at fixed locations in space and at discrete instants in time. The locations in space at which velocity and vorticity are measured usually form a rectangular grid of data points in the animal wake. The analysis of these wake measurements for force estimation currently proceeds in an *ad hoc* manner, specific to the animal being studied and the techniques used to measure the flow.

This paper aims to generalize and formalize the methodology of force estimation from wake measurements by addressing the following questions. What is the minimum number of wake properties whose combination is sufficient to determine swimming and flying forces from wake measurements? Does this set of wake properties change depending on the kinematics (e.g. unsteadiness, three-dimensionality) of the flow being studied? Can this set of wake properties be determined directly from Eulerian, DPIV-type data?

Answers to these questions will guide future empirical investigations in comparative biology and biological fluid mechanics, suggest limits to the capabilities of existing measurement techniques, and aid the development of new experimental methods.

Materials and methods

The relationship between flow and force

To establish a quantitative relationship between the fluid motions generated by a swimming or flying animal and the resultant locomotive forces, let us examine the balance of forces acting on the animal. In fluid dynamics, it is common to accomplish a force balance analysis like this by considering a control volume surrounding the animal (Fig. 1). The control volume is an imaginary boundary surrounding the body on which fluid forces are being exerted (or which is itself exerting force on the fluid). The control volume boundary should enclose both the body and the fluid with which it is interacting.

To simplify the present analysis, we will first assume that the animal is moving at a constant velocity. Hence, by moving the control volume along with the steadily translating animal, the control volume becomes stationary in the reference frame of the animal. In addition, the effect of fluid viscosity (subsequent to wake vortex formation) will be neglected in this analysis. The implications of this inviscid flow assumption will be discussed later in this paper. Finally, the fluid is assumed to be incompressible.

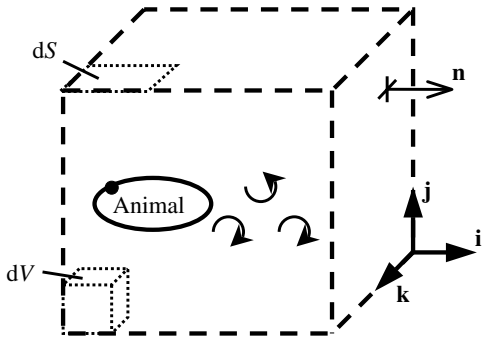

Fig. 1. Schematic of control volume concept, indicating variables described in the text. The control volume moves along with the animal so that it is stationary in the reference frame of the animal. The boundary of the control volume encloses both the animal and the fluid with which it interacts. The vortex wake resulting from this interaction is shown trailing the animal. For definitions, see List of symbols.

Our goal is now to determine the rate at which the fluid momentum of the control volume changes. By Newton's second law, the rate at which the control volume fluid momentum changes is equal to the sum of the forces exerted on the fluid inside the control volume and on the surface of the control volume. The force balance implied by this statement of Newton's second law, combined with the aforementioned simplifying assumptions, can be expressed as (Smits, 2001):

$$\frac{\partial}{\partial t}\int \rho \mathbf{u}\,\mathrm{d}V + \int (\mathbf{n}\cdot\rho\mathbf{u})\,\mathbf{u}\,\mathrm{d}S = \int \mathbf{n}p\,\mathrm{d}S + \mathbf{F}. \quad (1)$$

In Eq. 1, $\mathbf{u}$ is the Eulerian velocity field. $\mathbf{u}(x,y,z,t)=u\mathbf{i}+v\mathbf{j}+w\mathbf{k}$, where u, v and w are the flow velocity components (i.e. flow speeds) in the x, y and z directions, respectively, and $\mathbf{i}$, $\mathbf{j}$ and $\mathbf{k}$ are unit vectors (i.e. vectors of magnitude equal to one) in the x, y and z directions, respectively (see Fig. 1 for orientation). The variable $\mathbf{n}$ is a unit vector oriented normal to each portion dS of the surface of the control volume and pointing out of the control volume. The fluid density and pressure are represented by the variables ρ and p, respectively. Finally, the vector $\mathbf{F}$ is the net force exerted on the fluid inside the control volume.

The first term in Eq. 1 is the rate of change of fluid momentum inside the control volume. The partial derivative, $\partial/\partial t$, indicates that although the integrand $\rho\mathbf{u}$ is potentially a function of space (i.e. x, y and z) and time, we are only concerned with its temporal variations. The second term is the rate at which fluid momentum is transported out of the control volume, with the sign of this term being positive when the velocity vector is oriented in the direction of the unit normal vector $\mathbf{n}$ (i.e. an outflux of momentum). The sum of these two terms is the net rate of change of control volume fluid momentum.

Forces acting on the control volume can be exerted either at the surface or inside the control volume. The surface forces are accounted by integrating the fluid pressure on the entire surface of the control volume, i.e. the first term on the right-hand side of Eq. 1. Since the animal is the only body in the fluid, we know that it is responsible for the force **F** acting inside the control volume.

By Newton's third law, the animal experiences a reaction force –**F** in response to the force it applies to the fluid. It is this reaction force that drives locomotion. Thus, in principle, the instantaneous, time-dependent fluid dynamic force that facilitates swimming and flying motions can be deduced from the fluid flow by using the equation:

$$\mathbf{F}(t) = \int \mathbf{n} p \mathrm{d}S - \frac{\partial}{\partial t}\int \rho \mathbf{u} \mathrm{d}V - \int (\mathbf{n}\cdot\rho\mathbf{u})\,\mathbf{u}\mathrm{d}S\,, \qquad (2)$$

where t is time.

The benefit of this type of control volume analysis is that the exact details momentum transfer and force generation are not needed. However, the equation of motion (Eq. 2) dictates that the Eulerian velocity field **u** is not sufficient by itself to determine the forces generated by swimming and flying animals using this control volume method; the fluid pressure p is also required. As mentioned previously, this is a difficult task to accomplish with existing experimental techniques.

The control volume analysis and associated velocity/pressure perspective are limited in other critical points as well. For example, the control volume must be large enough to enclose all fluid whose momentum is affected by the animal. Even if one could determine a boundary for this region of affected fluid, the limited size of the measurement window in experiments makes it unlikely that all of this fluid could be measured simultaneously. Furthermore, in cases when an animal exhibits linear or angular accelerations, a proper control volume cannot be defined since the measured forces will change in an accelerating frame of reference. These constraints severely limit the applicability of the control volume approach in animal studies, and are a primary reason for the lack of velocity/pressure-based control volume analyses in the animal locomotion literature.

The vorticity perspective

The difficulties described above suggest that we search for other wake properties that allow us to deduce changes in wake momentum and, hence, to determine corresponding force generation during animal swimming and flying. One such property is the vorticity, a measure of rotation and shear (i.e. spatial velocity gradients) in the fluid. The momentum in the wake is manifested in the vorticity field **ω**. It can be computed by taking the mathematical curl (denoted $\nabla\times$) of the velocity field:

$$\boldsymbol{\omega} = \nabla\times\mathbf{u} = \left(\frac{\partial w}{\partial y} - \frac{\partial v}{\partial z}\right)\mathbf{i} - \left(\frac{\partial w}{\partial x} - \frac{\partial u}{\partial z}\right)\mathbf{j} + \left(\frac{\partial v}{\partial x} - \frac{\partial u}{\partial y}\right)\mathbf{k}\,. \qquad (3)$$

Saffman (1992, chapters 3–5) derived a quantitative relationship between the vorticity field and the net force exerted on the fluid in order to generate the vorticity:

$$\mathbf{F} = \rho\frac{\partial}{\partial t}\int \mathbf{x}\times\boldsymbol{\omega}\mathrm{d}V_{\mathrm{V}} + \rho\frac{\partial}{\partial t}\int \boldsymbol{\phi}\mathbf{n}\mathrm{d}S_{\mathrm{V}}, \qquad (4)$$

where **x** is the position of the vector (relative to a pre-defined origin) of each fluid particle in the flow (Fig. 2).

The integrals in Eq. 4 are evaluated throughout the volume V_{V} and over the surface S_{V} of the region of flow containing vorticity, i.e. the wake vortices (Fig. 2). These vortices need not be stationary as in the case of the control volume previously examined. Note that we also no longer need to contend with the pressure term directly, as it is eliminated in the process of deriving Eq. 4. However, a new velocity potential term **ϕ** appears. Physically, the velocity potential is related to the fluid pressure *via* the unsteady Bernoulli equation:

$$\frac{\partial\boldsymbol{\phi}}{\partial t} + \frac{1}{2}(\nabla\boldsymbol{\phi})^2 \approx C(t) - \frac{p}{\rho}\,, \qquad (5)$$

where C (Bernoulli variable) is dependent on time t and any external forces acting on the fluid. The approximation sign has been used because equality only holds if the force **F** in Eq. 4 is conservative (i.e. it does not dissipate energy). This cannot always be guaranteed for the forces generated by swimming and flying animals. The velocity potential term in Eq. 4 is non-zero in any flow that exhibits sufficient unsteadiness to create a net fluid circulation in the wake during a finite period of time. The velocity potential contribution only vanishes for a steady flow in which the spatial distribution of vorticity does not change in time. This restriction is unrealistic for most modes of animal swimming and flying, since it is typical for net circulation to be constantly shed into the wake.

We now have two complementary perspectives for estimating locomotive forces from wake measurements: velocity/pressure (**u**–p) and vorticity/velocity potential (**ω**–**ϕ**). The benefit of the velocity potential term relative to pressure

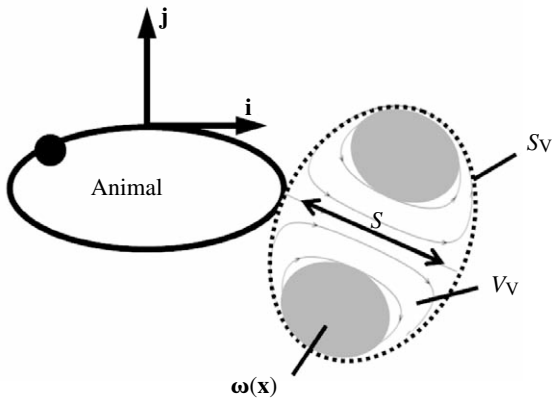

Fig. 2. Schematic of wake vortex parameters described in the text. The distribution of wake vorticity **ω**(**x**) is indicated by grey patches in this cross-section view. Hypothetical flow streamlines inside the vortex are sketched below the vortex patches. The integrals in Eq. 4 are evaluated throughout the vortex volume V_{V} and on the vortex surface S_{V}. The dimension S is the wake vortex width.

is that a simple and robust method exists to determine its magnitude from velocity data, unlike the fluid pressure. The following section describes this method.

A connection between velocity potential and wake vortex added-mass

As mentioned in the previous section, a force contribution from the velocity potential exists in the form of an integral evaluated over the surface of the wake vortices (Fig. 2). Importantly, it has been previously noted that the surface integral of a velocity potential such as that in Eq. 4 is equal to the added-mass associated with the body enclosed by the surface (e.g. Benjamin, 1986; Saffman, 1992). However, the surface in Eq. 4 encloses fluid, i.e. the wake vortex. Can the relationship between velocity potential and added-mass hold for a fluid body such as a vortex in the same manner that it does for solid bodies?

The literature on the physics of added-mass is relatively sparse, with a few notable exceptions (e.g. Darwin, 1953; Batchelor, 1967; Daniel, 1984; Eames et al., 1994, 1997; Bush and Eames, 1998; Eames and Flor, 1998; Eames, 2003). Qualitatively, the concept of added-mass accounts for the resistance force that a body faces when it is accelerated through a surrounding medium of non-zero density. The surrounding medium can be any fluid, e.g. air, water or blood. The surrounding medium need not have viscosity, so the analysis can proceed under an assumption of inviscid flow as in the preceding developments.

The resistance force occurs because, as the body moves forward, the surrounding medium interacts with the body at their interface (*via* the pressure field), ultimately leading to a net translation of the surrounding medium in the same direction as the traveling body. Hence, the force required to accelerate a body though a medium of non-zero density must overcome both the inertia of the body itself and the inertia of the surrounding medium that moves along with the body. This is the added-mass effect.

The added-mass contribution for uniform linear acceleration of a body can be expressed quantitatively by rewriting Eq. 4 as:

$$\mathbf{F}_{\mathrm{T}} = \rho_{\mathrm{B}}\Omega_{\mathrm{B}}\frac{\partial \mathbf{U}}{\partial t} + \rho_{\mathrm{M}}\frac{\partial}{\partial t}\int \phi \mathbf{n}\,\mathrm{d}S_{\mathrm{B}} = \Omega_{\mathrm{B}}(\rho_{\mathrm{B}}+\rho_{\mathrm{M}}\mathbf{C}_{\mathrm{AM}})\frac{\partial \mathbf{U}}{\partial t}, \quad (6)$$

where $\mathbf{F}_{\mathrm{T}}$ is the total force required to accelerate (at a rate $\partial\mathbf{U}/\partial t$) a body of volume Ω_{B} and density ρ_{B} through a surrounding medium of density ρ_{M} (Saffman, 1992). The variable $\mathbf{C}_{\mathrm{AM}}$ is the added-mass tensor, a 3×3 matrix whose elements c_{ij} are the dimensionless added-mass coefficients that relate linear acceleration in the ith direction to the resultant forces in the jth direction (where i and j can assume the x-, y- and z-axis directions, and repeated subscripts c_{ii} do not indicate summation):

$$\mathbf{C}_{\mathrm{AM}} = \begin{bmatrix} c_{\mathrm{xx}} & c_{\mathrm{xy}} & c_{\mathrm{xz}} \\ c_{\mathrm{xy}} & c_{\mathrm{yy}} & c_{\mathrm{yz}} \\ c_{\mathrm{xz}} & c_{\mathrm{yz}} & c_{\mathrm{zz}} \end{bmatrix}. \quad (7)$$

The variable $\partial\mathbf{U}/\partial t$ is a 3×1 vector whose elements U describe the linear acceleration of the body in the x-, y- and z-axis directions, respectively:

$$\frac{\partial \mathbf{U}}{\partial t} = \begin{bmatrix} \partial U_{\mathrm{x}}/\partial t \\ \partial U_{\mathrm{y}}/\partial t \\ \partial U_{\mathrm{z}}/\partial t \end{bmatrix}. \quad (8)$$

It is important to note that the full motion of the body is described by larger added-mass and acceleration tensors (with dimensions 6×6 and 6×1, respectively) that also account for rotational acceleration of the body in the xy-, xz- and yz-planes and the associated moments (torques) on the body (cf. Batchelor, 1967). In general these rotational components should not be assumed to be negligible. However, for the purpose of demonstration in this paper, it is sufficient to focus on the linear acceleration components.

The contribution of the added-mass of the body to the force required to accelerate it will depend on the body shape and the type of motion it is experiencing (i.e. which components of the added-mass tensor are relevant), as well as the relative densities of the body and the surrounding medium. For example, the force $\mathbf{F}_{\mathrm{A}}$ required to accelerate an axisymmetric body (with respect to the x-axis) along the x-axis through a surrounding medium of density equal to the body is given by:

$$\mathbf{F}_{\mathrm{A}} = \rho\Omega_{\mathrm{B}}\left(1+\begin{bmatrix} c_{\mathrm{xx}} & 0 & 0 \\ 0 & c_{\mathrm{yy}} & 0 \\ 0 & 0 & c_{\mathrm{zz}} \end{bmatrix}\right)\begin{bmatrix} \partial U_{\mathrm{x}}/\partial t \\ 0 \\ 0 \end{bmatrix} = \rho\Omega_{\mathrm{B}}(1+c_{\mathrm{xx}})\frac{\partial U_{\mathrm{x}}}{\partial t}\mathbf{i}. \quad (9)$$

The only physical properties required of the accelerating body are that it possesses a non-zero density and that it has a physical boundary separating it from the surrounding flow. This boundary redirects particles in the surrounding medium (*via* the pressure field) so that they pass around the body, ultimately leading to the net translation of the surrounding medium in the direction of body motion. As mentioned previously, this net translation of the surrounding medium is the source of the added-mass contribution. The body may be solid such as a wing, fin or heart valve; or fluid such as air, water or blood. However, in the latter case of fluid bodies, defining the boundary between the body and the surrounding medium is not an obvious task.

The Eulerian velocity field generally does not indicate the presence of fluid bodies or their boundaries in the flow. Dabiri and Gharib (2004) illustrated this difficulty for the case of mechanically generated vortex rings. In this case, the wake is formed by a piston that accelerates fluid through the open end of a hollow tube. As the boundary layer vorticity that formed inside the tube is ejected downstream from the open end, it rolls into a vortex ring that propagates though the surrounding fluid.

When DPIV measurements of the flow are presented as a

vector field or as streamlines (i.e. lines tangent to the field of velocity vectors throughout the flow), there is no indication of a boundary between fluid particles recirculating in the vortex and those redirected around the vortex (Fig. 3A). However, if the same data is plotted in a reference frame moving with the vortex ring (i.e. by adding the forward velocity of the vortex ring to every velocity vector in the flow field), we can identify the boundary of the vortex with reasonable accuracy (Fig. 3B).

Fluid particles inside the vortex recirculate, while fluid particles outside the vortex are redirected around boundary in the same manner as flow around an equivalent solid body. Interestingly, the vortex boundary does not form a toroid as suggested by the vorticity field, but instead takes an ellipsoidal shape. In a later section of this paper, measurements will demonstrate that an added-mass is indeed associated with this fluid vortex, and that the magnitude of the added-mass contribution is equal to that of a solid body with the same boundary dimensions.

The preceding discussion does not yet resolve the issue of how to determine the boundary of vortices in animal wakes so that we may quantitatively evaluate their added-mass contribution, e.g. by using Eq. 4. The transformation of reference frame utilized by Dabiri and Gharib (2004) is limited to simple flows such as a train of mechanically generated vortex rings. It is not clear that an extension of their reference frame transformation method to the more complex vortex wakes of swimming and flying animals is possible.

It has recently been demonstrated that by tracking the motion of individual fluid particles in the flow instead of analyzing the entire velocity field at each instant in time (i.e. the Eulerian perspective), it is possible to quantitatively determine the boundaries of vortices in a measured flow without changing the frame of reference of the measurements (S. C. Shadden, J. O. Dabiri and J. E. Marsden, manuscript submitted for publication). The method of Shadden et al. exploits the fact that, regardless of the frame of reference, vortex boundaries are known to separate fluid particles that recirculate inside the vortices from fluid particles that are redirected around the vortices. Given the wake vortex boundaries, we are left with the challenge of empirically

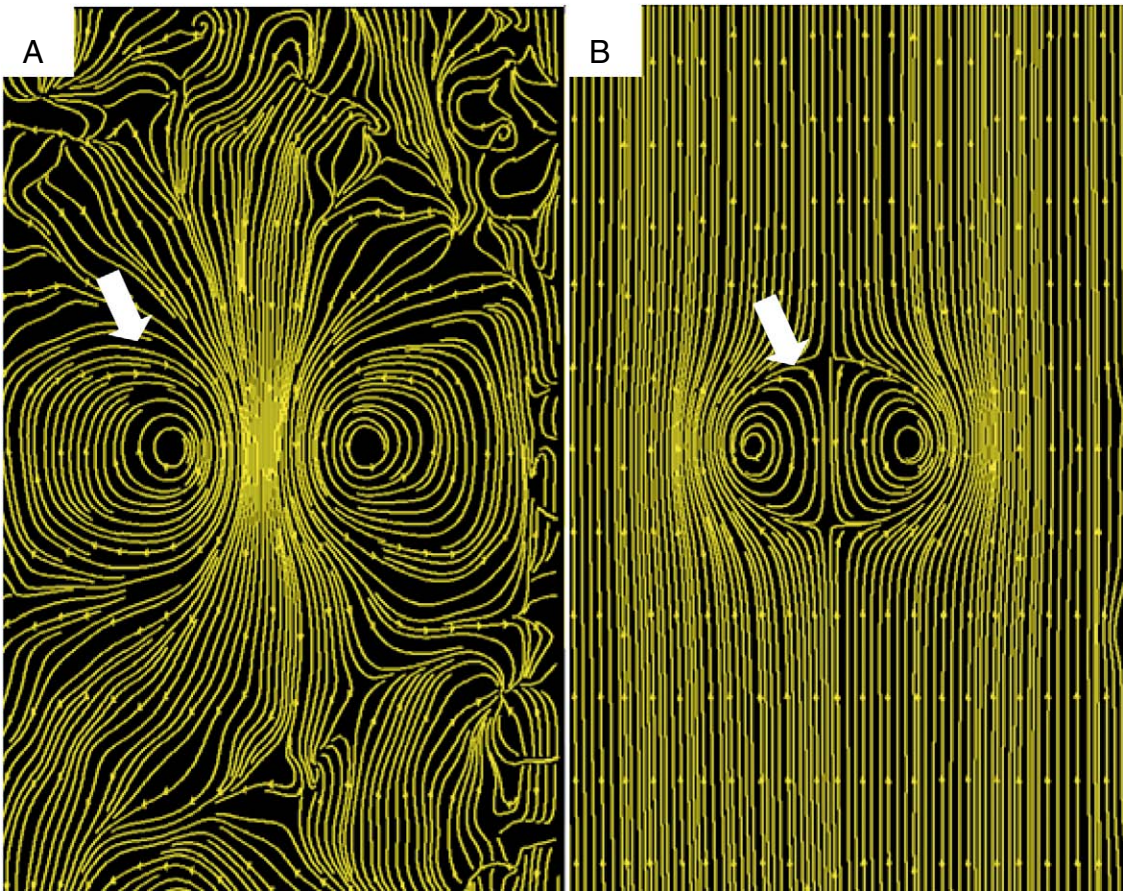

Fig. 3. DPIV measurements of flow created by a mechanical wake generator. Images correspond to a meridian symmetry plane of the wake vortex ring. Streamlines of the velocity field (i.e. lines tangent to each vector in the velocity field) are plotted in yellow. Exit plane of the vortex generator is located at the upper margin of the frame. Flow is directed vertically downward. Flow field is 20 cm in height. (A) View of vortex ring propagating downstream from the mechanical wake generator in the laboratory reference frame. (B) Same vortex ring as in A, viewed in a reference frame that moves at the speed of the propagating vortex ring. The full extent of the vortex is clearly visible from this perspective. White arrows indicate location of vortex ring in A and B.

measuring the added-mass of the wake vortices (i.e. the second term on the right-hand side of Eq. 4) and determining the magnitude of the wake vortex added-mass contribution to the forces generated by swimming and flying animals.

Measuring the wake vortex added-mass contribution

The physical description of the added-mass concept in the previous section suggests that to compute its effect in vortex wakes, we must examine the dynamics of fluid surrounding the wake vortices. Conveniently, Darwin (1953) developed a simple method that quantitatively connects the translation of fluid outside of a body (e.g. the fluid vortex body of present interest) to the added-mass of the body itself. To quantitatively track the translation of the fluid surrounding the vortex, it is convenient to replace the Eulerian perspective that examined the entire velocity field at single instances in time with a Lagrangian approach that tracks the trajectories of individual particles of the fluid over long durations of time. Conveniently, the Lagrangian description of the flow can be derived from the Eulerian velocity field.

To do so, let us imagine that a particle of the fluid surrounding the vortex is located at the position $\mathbf{x}_0=x_0\mathbf{i}+y_0\mathbf{j}+z_0\mathbf{k}$ at time t_0. The Eulerian velocity field dictates that a fluid particle at that position at that time has a velocity $\mathbf{u}(\mathbf{x}_0,t_0)$. Hence, a small time later, $t_1=t_0+\Delta t$, the particle will have the new position $\mathbf{x}_1$, where:

$$\mathbf{x}_1 \approx \mathbf{x}_0 + \mathbf{u}(\mathbf{x}_0,t_0)\Delta t \,. \qquad (10)$$

The velocity of the fluid particle at the new position $\mathbf{x}_1$ and at time t_1 will be given by the Eulerian velocity $\mathbf{u}(\mathbf{x}_1,t_1)$. This information can be used to update the particle position to $\mathbf{x}_2$, and so on. The record of fluid particle trajectories $\mathbf{x}(t)$ such as this provides a Lagrangian description of the flow.

The method of Darwin (1953) uses the following Lagrangian method for determining the added-mass contribution. Suppose that a plane of initially stationary particles in the flow downstream of a body (such as our fluid vortex) that is traveling at constant velocity is tracked in order to determine the Lagrangian motion of the particles that is induced by the passage of the body (Fig. 4). The volume of surrounding fluid that is enclosed between the initial plane of particles and the distorted plane that results after the body has passed far downstream (called the drift volume Ω_D) is equal to the product of the volume of the body Ω_B and the added-mass coefficient c corresponding to the direction of body travel, i.e.

$$c_{ii} = \frac{\Omega_{Di}}{\Omega_B} \,, \qquad (11)$$

where i=x, y or z.

A similar method can be used to determine the added-mass coefficients corresponding to the case of a body in rotational motion (Darwin, 1953).

Fig. 4 illustrates the method of Darwin (1953) by computing the Lagrangian fluid particle trajectories of flow surrounding a solid sphere that travels along the x-axis at constant velocity through an inviscid fluid. This flow is an exact solution derived

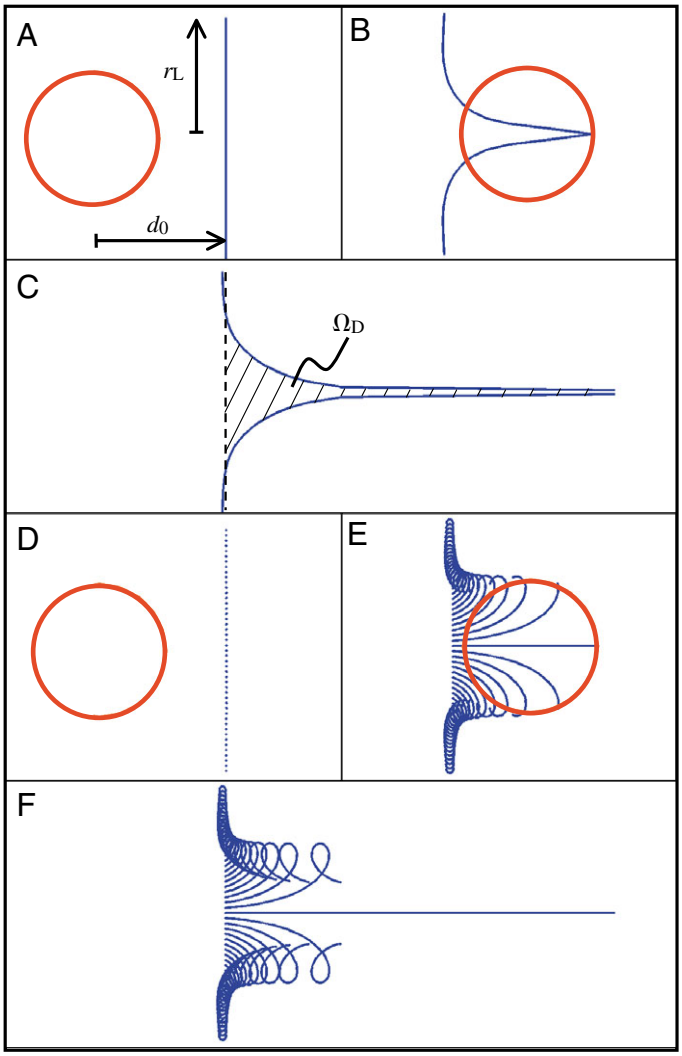

Fig. 4. Demonstration of the method for measuring solid body added-mass (i.e. Darwin, 1953). Axisymmetric inviscid flow about a solid sphere is shown in cross section. Solutions were computed using dimensional units to allow comparison with experimental results. Sphere radius and propagation speed are 2.54 cm and 1 cm s^{-1}, respectively. Computational domain is 50 sphere radii axially in both directions normal to the reference plane and approximately 12 cm radially. Variables d_0 and r_L indicate (qualitatively) finite upstream approach distance and reference plane radius, respectively. Total fluid drift (i.e. for infinite domain) was computed using measured partial drift in the computational domain and an analytical asymptotic correction factor (i.e. Eq. 12; Eames et al., 1994). (A) Sphere approaches initially planar Lagrangian surface from left; t=0 s. (B) Streamwise distortion of Lagrangian surface occurs as the sphere passes through the plane; t=4.45 s. Note that since only streamwise Lagrangian displacement is plotted, the sphere appears to pass through the plane. Plots of combined streamwise and transverse Lagrangian displacement (e.g. D–F below) verify that the plane is actually distorted around the sphere. (C) Volume between initial plane and horn-like distorted surface is the drift volume, Ω_D, from which the added-mass coefficient is computed; t=13.3 s. (D–F) Individual Lagrangian particle paths corresponding to t=0 s, 4.45 s and 13.3 s, respectively.

from the fluid dynamic equations of motion (Milne-Thomspon, 1968). The volume of surrounding fluid enclosed between the initial plane of particles and the horn-shaped distorted plane that results after the solid body has passed far downstream is equal to one-half of the sphere volume. This is consistent with the known added-mass coefficient for translation of a solid sphere, i.e. c_{xx}=1/2.

Note that although the body has a simple motion and the streamlines of the flow past the body would suggest similarly simple fluid particle trajectories, this is not the case. Rather than the particle motion being uniform over time, fluid particles exhibit looping trajectories called elasticas (Fig. 4). During each elastica trajectory, a fluid particle briefly travels in the direction opposite to the body translation. These particle kinematics are reflected in a plot of the drift volume *vs* time (Fig. 5), in which an oscillation occurs before the drift volume saturates at a constant value. Furthermore, although the net motion of fluid surrounding the body is in the direction of the traveling body, the motion of the surrounding fluid does not occur uniformly in space. Regions of the fluid closer to the body experience a greater net translation. As one would expect, the net translation of each fluid particle in the surrounding flow is less than or equal to the net translation of the body itself.

These details are missed in an analysis of the Eulerian velocity field, but are critical for understanding the kinematics and dynamics of the added-mass associated with fluid bodies such as wake vortices, as will be seen in the following section.

Extension of Darwin's added-mass method to wake vortices

Given the idealized nature of the added-mass measurement technique developed by Darwin, care must be taken in extending it to flows of practical concern such as the wakes of swimming and flying animals. The proof presented by Darwin (1953) and others for the validity of the added-mass measurement technique described above is limited to the case of solid bodies moving in an infinite expanse of fluid. More recent work by Eames et al. (Eames et al., 1997; Bush and Eames, 1998; Eames and Flor, 1998; Eames, 2003) suggests that the method of Darwin can be extended to include more realistic flows where the extent of the surrounding fluid is finite, and to include the case of fluid bodies such as vortices in air and water moving through a surrounding fluid of equal density.

To address the issue of a finite surrounding flow volume, Eames et al. (1994) introduced the concept of partial drift to describe drift volume measurements in which the body travels only a finite distance through the plane of Lagrangian particles being tracked. The concept of partial drift also accounts for the fact that the size of the plane of Lagrangian particles is limited by the measurement window size, and therefore cannot be infinite in practice as Darwin's method assumes. An approximate relationship between the partial drift volume $\Omega_{D,partial}$ measured in practice and the total drift volume Ω_D required in the analysis of Darwin (1953) is given by:

$$\frac{\Omega_{D,partial}}{\Omega_D} \approx -\frac{1}{2} + \left(\frac{3}{2\sqrt{1+(r_L/d_0)^2}} \right), \qquad (12)$$

where r_L is the (finite) radius of the plane of Lagrangian fluid particles being tracked and d_0 is the (finite) distance upstream from the Lagrangian plane at which the motion of the body toward the plane is initiated (Eames et al., 1994; see also Fig. 4A). Although this equation is strictly valid only for spherical wake vortices, we will see that it also provides a useful approximation for a wider class of vortex wake geometries as well.

Given the vorticity/velocity-potential Eq. 4, the connection between velocity-potential and wake vortex added-mass (Eq. 6), the added-mass measurement technique of Darwin (Eq. 11), and the concept of partial drift (Eq. 12), we are now prepared to develop an improved method to estimate swimming and flying forces based on wake measurements, especially the types of data available from DPIV.

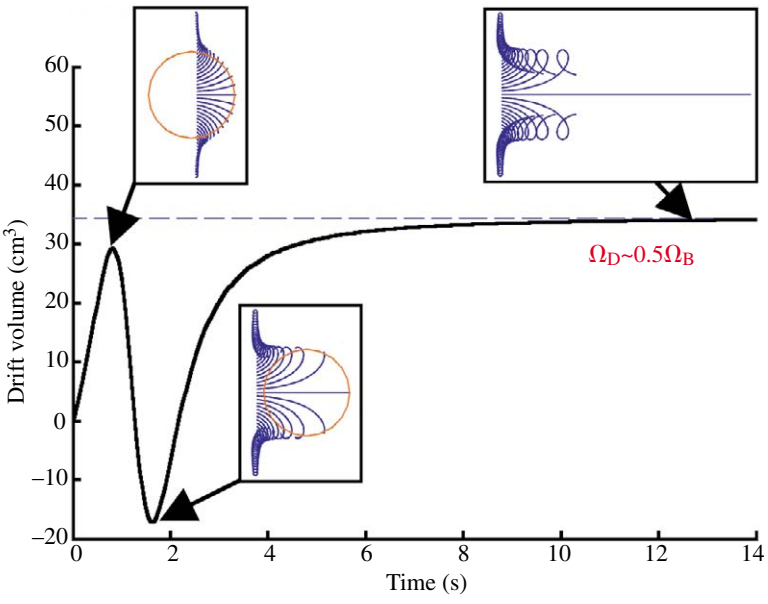

Fig. 5. Time dependence of drift volume induced by the motion of a solid sphere through an inviscid fluid. Sphere radius and propagation speed are 2.54 cm and 1 cm s^{-1}, respectively. Total fluid drift (i.e. for infinite domain) was computed using measured partial drift in the measurement window and an analytical asymptotic correction factor (i.e. Eq. 12; Eames et al., 1994). The oscillation in drift volume corresponds to changes in direction of Lagrangian particle translation during looping elastica trajectories.

As a first step we must determine the added complexity that arises due to a fluid body such as a wake vortex in air or water moving in a surrounding fluid of equal density. To do so, the same Lagrangian particle analysis performed using the theoretical inviscid flow past a sphere (i.e. Fig. 4) is accomplished, this time by using DPIV measurements of a mechanically generated wake of vortex rings. The wake vortex rings were generated using a piston-cylinder apparatus (Dabiri and Gharib, 2004), which was submerged in water and ejected discrete pulses of fluid with jet length-to-diameter ratio L/D=2 from the open end of a hollow 2.54 cm diameter circular tube. During each pulse, the vorticity shed by the wake generator rolled into a single ring vortex that propagated downstream *via* its self-induced motion. The downstream velocity field created by the wake generator was measured by using DPIV with an uncertainty between 1% and 3%. Larger uncertainty occurred in regions with greater spatial velocity gradients. Lagrangian particle trajectories of several axisymmetric planes downstream of the wake generator, each with 4.5 cm radius and unit normal vector **n** aligned with the direction of wake vortex translation, were quantitatively tracked using the method of Eq. 10. The partial drift of each plane of Lagrangian particles was measured from this data.

Results

Wake vortex added-mass measurements

Lagrangian particles in the mechanically generated vortex wake were observed to behave in a manner very similar to the inviscid sphere solution (compare Figs 4 and 6). Looping elastica paths were induced by each translating vortex, and the initially planar surfaces were again distorted to horn-like shapes.

Fig. 7 plots the drift volume measured for several planes of initially stationary Lagrangian particles located downstream of the wake generator. The drift volume of the sphere in inviscid fluid from Fig. 4 above is included for comparison. Whereas the drift volume associated with the sphere reaches a maximum value equal to one-half the sphere volume (consistent with the known added-mass coefficient of a sphere, c_{xx}=1/2), the drift volume of the wake vortex continually increases.

The continuous growth of the drift volume reflects the concomitant growth of the wake vortex due to fluid entrainment. Entrainment is the process whereby fluid surrounding the wake vortex is engulfed into the vortex itself, leading to the observed increase in the wake vortex volume (Dabiri and Gharib, 2004). Since the magnitude of the drift volume is a function of the body volume (*via* the added-mass coefficient; cf. Eq. 11), the drift volume also increases due to fluid entrainment by the wake vortex.

Therefore, in the case of wake vortices, rather than the added-mass coefficient reflecting the ratio of the drift volume magnitude to the body (i.e. wake vortex) volume magnitude, it indicates the ratio of the drift volume growth rate to the body volume growth rate, i.e.

$$c_{ii} = \frac{\left(\frac{d\Omega_{Di}}{dt}\right) - \left(\frac{d\Omega_{E}}{dt}\right)}{\left(\frac{d\Omega_{V}}{dt}\right)}, \qquad (13)$$

where $d\Omega_V/dt$ *is* the vortex volume growth rate and $d\Omega_E/dt$ is the volume of surrounding fluid entrained into the vortex per unit time. Note that we must subtract the volume of entrained

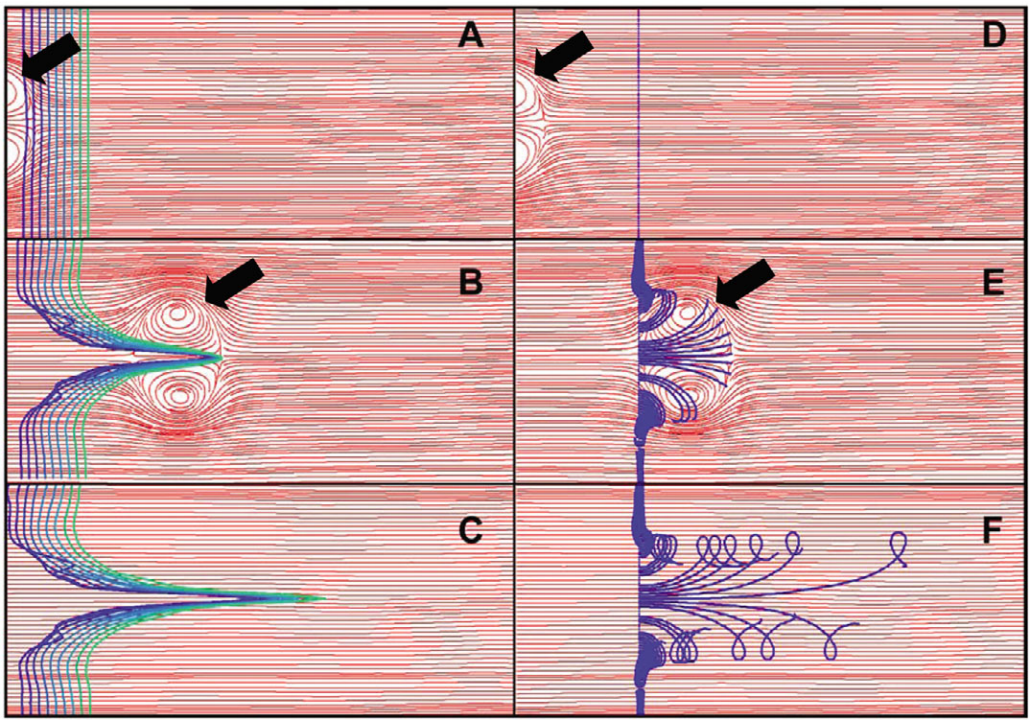

Fig. 6. Measurements of Lagrangian drift induced by translating fluid vortices. Vortex is indicated by black arrow. (A) Vortex approaches several planar Lagrangian surfaces downstream of the vortex generator (several more planes further downstream not shown); t=0.07 s. (B,C) Fluid vortices interact with Lagrangian surfaces in a manner similar to that observed for the inviscid sphere solution. Initially planar surfaces are deformed to horn-like shapes; t=3.34 s and 13.3 s, respectively. (D–F) Individual Lagrangian particle paths corresponding to t=0.07 s, 3.34 s and 13.3 s, respectively.

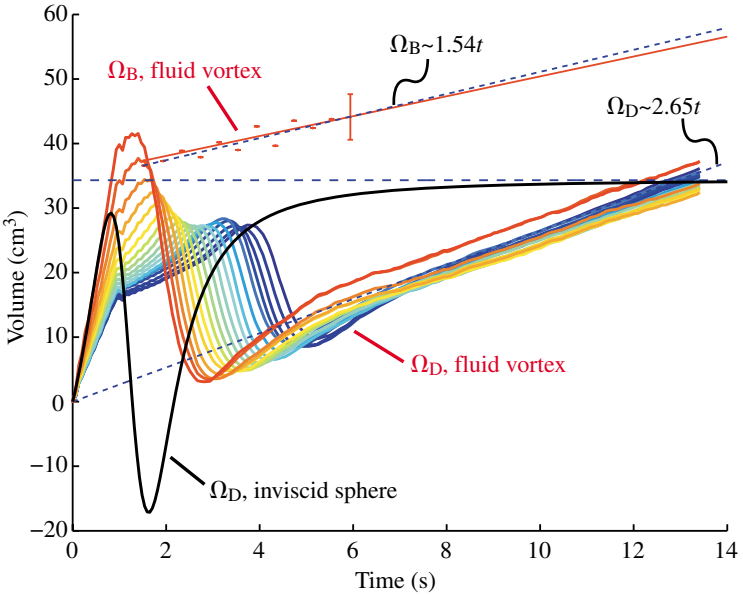

Fig. 7. Drift and fluid body volume measurements for translating vortices. Colored solid lines: drift volume of planes initially located in 0.3 cm increments from 2.7 cm (red) to 8.0 cm (blue) downstream of the vortex generator exit. Total fluid drift (i.e. for infinite domain) was computed using measured partial drift in the measurement window and an analytical asymptotic correction factor (i.e. Eq. 12; Eames et al., 1994). Closed circles: measured volume of ellipsoidal fluid vortex. Error bars indicate measurement uncertainty. Broken blue line: least-squares linear fit to vortex volume measurements. Solid red line: linear fit required to exactly match the added-mass coefficient of an equivalent solid body. Inviscid sphere solution is plotted for comparison (black line).

fluid from the drift volume in Eq. 13 since it is automatically included in the wake vortex volume Ω_V.

Applying this analysis to the experimental data from the mechanical wake generator, the added-mass coefficient c_{xx} of the mechanically generated wake vortices is:

$$c_{xx} = \frac{2.65\,\text{cm}^3\text{s}^{-1} - 1.54\,\text{cm}^3\text{s}^{-1}}{1.54\,\text{cm}^3\text{s}^{-1}} = 0.72\,. \qquad (14)$$

This is precisely the added-mass coefficient of a solid ellipsoid with the same shape as the mechanically generated wake vortices, where the wake vortex shape was determined using the frame transformation method of Dabiri and Gharib (2004) described earlier. In Fig. 7, the least-squares linear fit to the vortex volume data is compared with the linear trend required for an exact match to the added-mass coefficient of an equivalent solid body. The agreement is very good, with the discrepancy being less than the experimental uncertainty (indicated by error bars).

An important principle underlying this result is that even though wake vortices will tend to increase in size due to fluid entrainment, their added-mass can be determined in a manner similar to that of solid bodies as long as the shape of the fluid body does not change significantly.

An improved force estimation method

Eq. 4 properly incorporates both the process of vorticity generation and rearrangement (*via* the first term) and the interaction of wake vortices with surrounding fluid (i.e. the added-mass effect *via* the second term) in the estimation of swimming and flying forces from wake measurements. However, the spatial and temporal resolution of input data required to evaluate Eq. 4 directly can limit its practical application, hindering the analysis of data collected by empirical methods such as DPIV. Given the results of the preceding section, we can develop an improved force estimation method that does not require the level of measurement resolution (temporal and spatial) required to evaluate the terms in Eq. 4 directly, but still captures each of the important physical contributions to swimming and flying forces including the wake vortex added-mass.

To accomplish this, let us approximate the first term in Eq. 4 in the manner that is common in the literature:

$$\rho\frac{\partial}{\partial t}\int \mathbf{x}\times\boldsymbol{\omega}\,\mathrm{d}V_V \approx \rho\frac{\mathrm{d}}{\mathrm{d}t}\,(A\Gamma)\,. \qquad (15)$$

The assumption inherent to this approximation is that the vorticity in the wake vortex is arranged into thin, closed vortex loops, e.g. vortex rings and vortex chains. Each loop encloses an area A and has a circulation Γ. In practice, the wake vortices will not be thin; nevertheless, the approximation is used here for consistency with previous studies. The author suggests that an examination of the adequacy of this common adaptation should be undertaken in the future.

The second term is the wake vortex added-mass contribution, and can be approximated based on the added-mass coefficient, as well as the size and trajectory of each wake vortex as it is formed in the wake:

$$\rho\frac{\partial}{\partial t}\int \boldsymbol{\phi}\mathbf{n}\,\mathrm{d}S_V \approx \rho c_{ii}\frac{\mathrm{d}}{\mathrm{d}t}\,(\Omega_V \mathbf{U}_{Vi}), \qquad (16)$$

where $\mathbf{U}_{Vi}$ is wake vortex velocity in the i direction relative to the animal. In its present form, Eq. 16 is difficult to use because both the added-mass coefficient and the vortex volume can only be determined exactly by using three-dimensional flow data. Existing experimental techniques such as DPIV are limited to two-dimensional measurements.

We can circumvent this difficulty by implementing two approximations. First, the added-coefficient c_{ii} can be estimated based on a cross-sectional view of the animal wake corresponding to the bilateral symmetry plane of the animal

(cf. Fig. 2). Ideally, the boundary of the forming wake vortex in this plane should be determined using a Lagrangian method (such as that of S. C. Shadden, J. O. Dabiri and J. E. Marsden, manuscript submitted for publication). In the absence of such a technique, the vortex boundary can also be estimated based on the spatial extent of wake vorticity or the use of dye or aerosol visualizations. This two-dimensional approximation of the added-mass coefficient will be denoted $\overline{c_{ii}}$. The added-mass of a three-dimensional body is typically lower than an estimate based on its two-dimensional cross-section (Daniel, 1983). However, the overestimation of the added-mass coefficient by the two-dimensional approximation will be compensated in Eq. 16 by the underestimation of the vortex volume, which arises when the vorticity distribution is used to determine the vortex boundary (cf. Dabiri and Gharib, 2004).

The two-dimensional approximation of the wake vortex boundary can also be used to estimate the vortex volume, i.e.:

$$\Omega_V \approx AS\,, \tag{17}$$

where S is the width of each wake vortex determined from the cross-sectional view (see Fig. 2). As in the added-mass coefficient approximation, the determination of the vortex width should ideally be made using a Lagrangian technique such as that of Shadden et al. (2005); however, the width of the vorticity in each wake vortex can provide a rough estimate of this parameter.

Combining these approximations with Eq. 15 gives the desired force estimation equation:

$$\mathbf{F} \approx \rho \frac{\mathrm{d}}{\mathrm{d}t}(A\Gamma + \overline{c_{ii}} AS\mathbf{U}_{Vi}). \tag{18}$$

The wake measurements required to evaluate Eq. 18 can be deduced by using existing wake measurement techniques such as DPIV, with little additional data analysis. The vortex area A and circulation Γ are commonly measured in the existing literature; the wake vortex width S and vortex velocity $\mathbf{U}_{Vi}$ can be estimated from Eulerian velocity and vorticity field measurements of the wake vortex cross-section. The added-mass coefficient $\overline{c_{ii}}$ can be determined from an equivalent solid body calculation of the identified vortex boundary, or by using the Lagrangian method of Eq. 13.

To make the expression in Eq. 18 compatible with the format of typical wake measurements, the time derivative can be written in terms of data taken at discrete time points t_0, $t_1=t_0+\Delta t$, $t_2=t_0+2\Delta t$, etc.:

$$\mathbf{F}(t_0) \approx \rho\{[A(t_1)\Gamma(t_1) + \overline{c_{ii}} A(t_1)S(t_1)\,\mathbf{U}_{Vi}(t_1)] - [A(t_0)\,\Gamma(t_0) + \overline{c_{ii}} A(t_0)\,S(t_0)\,\mathbf{U}_{Vi}(t_0)]\} \Big/ \Delta t\,. \tag{19}$$

As Δt decreases to zero, Eq. 19 becomes an estimate of the instantaneous force generated by the swimming or flying animal. As Δt increases to T, the duration of the propulsive stroke, Eq. 19 becomes an estimate of the time-averaged locomotive force.

The effect of the additional vortex added-mass terms in Eq. 19 can be quite substantial, depending on the level of unsteadiness during wake formation. The following section introduces a simple dimensionless parameter to aid the *a priori* determination of whether the contribution of wake vortex added-mass should be considered in a particular study of animal swimming and flying dynamics.

The wake vortex ratio (Wa)

To determine whether the added-mass of wake vortices should be considered in a particular study of animal swimming and flying dynamics, we must determine the relative contribution of the second term in Eq. 18. Let us define a dimensionless parameter, the wake vortex ratio (denoted Wa), as the ratio of the wake vortex added mass-term in Eq. 18 to the vortex circulation term:

$$\mathrm{Wa} = \frac{\frac{\mathrm{d}}{\mathrm{d}t}(\overline{c_{ii}} AS\mathbf{U}_{Vi})}{\frac{\mathrm{d}}{\mathrm{d}t}(A\Gamma)}\,. \tag{20}$$

Since the vorticity generated during each stroke cycle is created during the propulsive stroke duration T, the time derivatives in Eq. 20 can be approximated as:

$$\mathrm{Wa} = \frac{\overline{c_{ii}} AS\mathbf{U}_{Vi}}{T} \times \frac{T}{A\Gamma}\,, \tag{21}$$

or

$$\mathrm{Wa} = \frac{\overline{c_{ii}} S\mathbf{U}_{Vi}}{\Gamma}\,. \tag{22}$$

Note that both the area A enclosed by the wake vortex and the time parameter T are eliminated from Eq. 22. Therefore, the calculation of the wake vortex ratio can be accomplished by using a single, two-dimensional measurement of the wake vortex cross-section. When the added-mass coefficient, wake vortex width, or vortex velocity relative to the body is large relative to the vortex circulation, the wake is sufficiently unsteady that the contribution from wake vortex added-mass (e.g. Eq. 19) must be considered. To be more precise, the following criterion is suggested:

$$\text{For} \quad \mathrm{Wa} \geq \epsilon_\Gamma\,, \quad \rho \frac{\partial}{\partial t} \int \boldsymbol{\phi}\mathbf{n}\mathrm{d}S_V \neq 0, \tag{23}$$

where ϵ_Γ is the experimental uncertainty of the circulation measurement. The physical requirement dictated by this criterion is that the wake vortex added-mass (i.e. the numerator of the wake vortex ratio) should be discernable above the noise level of the circulation measurement. If the magnitude of the wake vortex added-mass contribution is less than the uncertainty of the circulation measurement, than it cannot be distinguished from the measurement noise and can be neglected. In practice, wake vortex circulation can often be measured to within ±10% (with the possibility of higher or

lower accuracies depending on the animal under consideration, wake Reynolds number, etc.).

It is useful to connect the wake vortex ratio Wa with existing dimensionless parameters used to describe animal swimming and flying. This can be accomplished by first considering the physical units of the variables in Eq. 22. In particular:

$$\overline{c_{ii}} \sim [1]; \quad S \sim [l]; \quad \mathbf{U}_{Vi} \sim [l\, s^{-1}]; \quad \Gamma \sim [l^2 s^{-1}], \qquad (24)$$

where l and s indicate length and time units, respectively, and the constant 1 indicates a dimensionless term. The relationships in Eq. 24 indicate that the wake vortex ratio in Eq. 22 can be rewritten in terms of a characteristic frequency $\hat{f}$, length scale $\hat{l}$, and velocity $\hat{U}$:

$$\mathrm{Wa} = \overline{c_{ii}} \frac{[l][l\, s^{-1}]}{[l^2 s^{-1}]} = \overline{c_{ii}} \frac{[s^{-1}][l]}{[l\, s^{-1}]} = \overline{c_{ii}} \frac{\hat{f}\,\hat{l}}{\hat{U}}, \qquad (25)$$

or, equivalently

$$\mathrm{Wa} = \overline{c_{ii}} \hat{\mathrm{St}}, \qquad (26)$$

where $\hat{\mathrm{St}}$ is a generic Strouhal number. The symbol $\hat{\mathrm{St}}$ is used to distinguish this parameter from the more common Strouhal number St in the animal locomotion literature, which is based specifically on the swimming or flight speed of the animal as well as its stroke amplitude (e.g. Taylor et al., 2003).

Despite differences between the definitions of $\hat{\mathrm{St}}$ and St, their trends will be similar. In particular, as the Strouhal number increases, the effect of wake vortex added-mass becomes more significant. This result is consistent with the fact that the Strouhal number (as used in the animal locomotion literature) is a measure of the periodicity of the body motion; therefore, it can also serve as a surrogate measure of the periodicity of wake flow created by the body motion. Interestingly, the relationship between St and Wa that is implied by Eq. 26 suggests the possibility that the observed tuning of swimming and flying locomotion according to the Strouhal number St (Taylor et al., 2003) may in fact be the consequence of a primary intention to tune for wake vortex ratio Wa.

Discussion

The existence of fluid vortex added-mass

The fact that fluid vortices exhibit an added-mass effect similar to solid bodies should not be unexpected. It is indeed quite common in fluid dynamics to analyze the flow around solid bodies by replacing them with distributions of fluid vorticity that result in equivalent flow behavior. For example, the flow around a solid sphere in inviscid fluid, such as that computed in Fig. 4, can be exactly reproduced by replacing the sphere with a spherical Hill's vortex of the same radius (Batchelor, 1967). The Lagrangian particle tracking analysis that was accomplished for the solid sphere in Fig. 4 would result in identical flow kinematics (e.g. drift volume measurements) if the spherical Hill's vortex were similarly translated through the plane of Lagrangian particles.

The existence of an added-mass effect associated with the fluid vortices in animal wakes has been recognized for nearly 30 years, dating back to the work of Weihs (1977) on aquatic locomotion *via* pulsed jets. However in that study, it was assumed that the calculation of vortex ring added-mass should be made on a toroidal geometry to reflect the distribution of vorticity in the wake vortices. It was also assumed that the volume of the wake vortices remains constant. The recent work of Dabiri and Gharib (2004) and Shadden et al. (2005) demonstrates that the proper geometry to be modeled for vortex rings is a temporally increasing ellipsoidal volume of fluid — both vortical and irrotational — translating with the vortex. Regardless of these details of vortex geometry, the wake vortex added-mass effect elucidated by Weihs (1977) has been neglected in nearly all recent studies of animal swimming and flying (for an exception, see Sunada and Ellington, 2001), in spite of its well-established origins in classical fluid dynamics.

Implications for previous force estimation studies

Despite the present demonstration of a wake vortex added-mass contribution to animal swimming and flying forces, the fact remains that previous studies appear to have successfully matched wake-based force estimates with the expected forces needed to sustain flight or to overcome negative buoyancy (e.g. Drucker and Lauder, 1999; Spedding et al., 2003; Warrick et al., 2005). How is this possible if wake vortex added-mass was neglected?

One important difference between force estimates that can be achieved using the methods introduced here (e.g. Eq. 19) and those in the literature is that existing methods estimate time-averaged forces rather than the instantaneous forces. The use of the time-average occurs both explicitly, for example, when the locomotive forces are averaged over the duration of the propulsive stroke (e.g. Warrick et al., 2005); or implicitly, when the wake is examined far downstream (e.g. Spedding et al., 2003). This latter case is equivalent to taking the time-average because the far downstream wake represents the integrated effect of the unsteady vortex formation process that occurred at the upstream site of force generation by the swimming or flying appendages.

Daniel (1984) has shown that in the case of solid bodies, the time-averaged added-mass force contribution is cancelled out if the body exhibits symmetric (in space and time) acceleration and deceleration phases during periodic motions. The published data from previous animal swimming and flying studies is insufficient to infer a similar cancellation of the wake vortex added-mass contributions during the stroke cycle. However, this effect remains a plausible explanation for the apparent absence of a wake vortex added-mass force contribution to time-averaged force measurements.

The use of time-averaged forces inferred from wake measurements for the purpose of deducing animal swimming and flying dynamics appears reasonable at first sight, as the forces required to achieve lift or overcome negative buoyancy should be achieved by the animal over durations sufficiently

long that a time-averaged force can be computed. However, an estimation of the time-averaged force provides no information about the instantaneous swimming and flying forces. It is these instantaneous forces that dictate important dynamics of locomotion such as the trajectory, speed and efficiency of swimming and flying. Furthermore, it can be shown that a time-averaged force estimate based on wake measurements is not sufficient to prove that an animal is generating the locomotive forces necessary to sustain flight or maintain neutral buoyancy.

To see this, consider the three hypothetical force profiles in Fig. 8. These curves represent the records of net vertical force, $\mathbf{F}_V$–$m\mathbf{g}$, generated by three flying animals, where $\mathbf{F}_V$ is the vertical fluid dynamic force and $m\mathbf{g}$ is the (constant) weight of the body (the same example can be equally applied to swimming animals with no loss of generality). Each animal starts from the same altitude and a zero vertical velocity. All three animals also possess the same time-averaged vertical force (i.e. $\overline{\mathbf{F}_V}$–$m\mathbf{g}$=0), and therefore cannot be distinguished using methods of time-averaged force estimation in a comparative biological study. However the vertical flight speeds $V(t)$ and flight trajectories $Y(t)$ of the three animals are very different (Fig. 8).

The animal with constant zero force generation does not change its altitude over time (Fig. 8; solid black line). The two animals with sinusoidal time-dependent force profiles both change their altitude, but in opposite directions. The animal whose instantaneous net force is initially positive increases its altitude (Fig. 8, blue broken line), while the animal whose instantaneous net force is initially negative decreases its altitude (Fig. 8, red dotted line). This latter animal is not generating sufficient force to sustain flight. Indeed, from any finite altitude, it will eventually descend to the ground. Yet a time-averaged force estimate would suggest that the forces generated by this animal are sufficient to maintain flight indefinitely, since the time-averaged fluid dynamic force $\overline{\mathbf{F}_V}$ is equal to the weight $m\mathbf{g}$ of the animal. An estimate of instantaneous forces is required to achieve more effective comparative biological studies that are capable of making these types of distinctions.

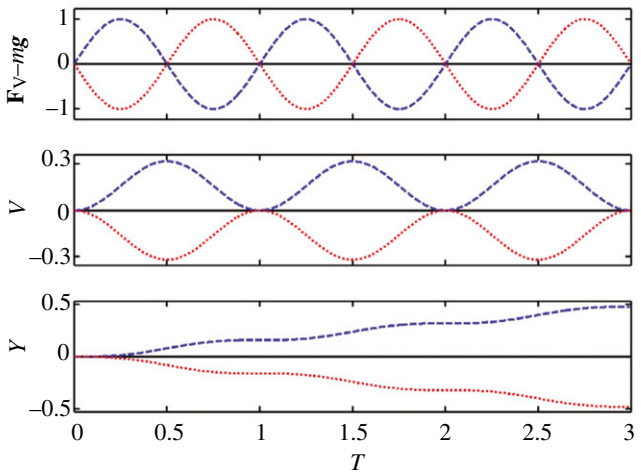

Fig. 8. Comparison of time-averaged and instantaneous forces and their related dynamics. Three hypothetical flying animals of equal weight ($m\mathbf{g}$) generate identical time-averaged forces but different instantaneous forces and flight dynamics over three stroke cycles. Solid black line, $\mathbf{F}_V$–$m\mathbf{g}$=0; broken blue line, $\mathbf{F}_V$–$m\mathbf{g}$=sin(2πt); dotted red line $\mathbf{F}_V$–$m\mathbf{g}$=–sin(2πt). Vertical velocity $V(t)$ and trajectory $Y(t)$ are determined from integration with initial conditions $V(0)$=0 and $Y(0)$=0. T, propulsive stroke duration. Figures are plotted using generic units.

The inadequacy of the time-averaged force for determining locomotive dynamics stems from the fact that the time-averaged force only dictates the behavior of the time-averaged acceleration, not the behavior of the time-averaged velocity or position of a body. For example, a time-averaged force equal to zero requires that (for a constant body mass) the time-averaged acceleration must also be equal to zero. The body must therefore start and end its motion at the same velocity. However, there is no implicit or explicit restriction on the velocity the body exhibits during the time between the start of the motion and its conclusion. An infinite set of temporal velocity profiles can be derived for the body, each one satisfying the requirement of zero time-averaged acceleration (and force). Consequently, the set of time-dependent position trajectories satisfying the requirement of zero time-averaged acceleration (and force) is also infinite.

A proper proof that an animal is generating sufficient locomotive forces to sustain flight or maintain neutral buoyancy requires knowledge of the instantaneous forces it is generating. The requirement that time-averaged forces generated by the animal should sustain flight or maintain neutral buoyancy is a necessary condition but it is not sufficient by itself.

These results indicate that even if instantaneous wake vortex added-mass forces exhibit no time-averaged contribution, they are still critical in determining the locomotive dynamics of swimming and flying animals.

Krueger and Gharib (2003) provide the only known comparison of instantaneous wake-measured force estimates with forces determined directly from a force balance device. The results of that work provide the best opportunity to compare the current experimental results with the existing literature, especially since both sets of experiments examine piston-generated vortex rings. In the current experiments, the wake vortex added-mass coefficient (c_{xx}=0.72), wake vortex width (S=3.2 cm), vortex velocity ($\mathbf{U}_{Vi}$=2 cm s^{-1}) and circulation (Γ=20 cm^2 s^{-1}) result in a wake vortex ratio (as defined in Eq. 22) Wa=0.23, suggesting that wake vortex added-mass provides a non-negligible contribution to the generated forces during vortex formation.

Unfortunately, the data presented by Krueger and Gharib (2003) is insufficient to compute the wake vortex ratio or to deduce the instantaneous forces generated early during vortex formation, when the contribution of wake vortex added-mass is expected to be the largest (i.e. due to vortex acceleration in the downstream direction). However, Krueger and Gharib (2003) do show that even after this period when wake vortex

added-mass is expected to be most significant, the impulse of the quasi-steady jet that forms behind the vortex is also underestimated by up to 10% when the contribution from wake vortex added-mass is neglected. The magnitude of force underestimation will become even more egregious during vortex formation. Hence, the results of Krueger and Gharib (2003) support the existence of a non-negligible contribution from wake vortex added-mass to the forces generated during wake formation. The present results suggest that the geometric picture of added-mass presented by Krueger and Gharib (2003) be revised, however. Rather than the wake vortex added-mass being distributed in a volume surrounding the vortex, Fig. 6 illustrates that it forms a horn of fluid that trails behind the translating vortex.

Implications for animal swimming and flying in general

As mentioned previously, the concept of wake vortex added-mass is not a discovery attributable to this paper; it is founded in classical fluid dynamics and has been appropriately recognized by a few investigators (e.g. Weihs, 1977; Krueger and Gharib, 2003). Furthermore, wake vortex added-mass is not a phenomenon that is specific to a particular vortex geometry such as the vortex rings studied in these experiments. The fluid dynamics concepts that dictate the existence of a wake vortex added-mass contribution are well established and generally applicable to any fluid flow containing vortices. It is therefore logical to hypothesize that wake vortex added-mass contributes to the dynamics of animal swimming and flying in general and, even more broadly, to vortex formation in any biological system including internal flows.

In the previous section, it was noted that since existing studies have focused on time-averaged forces, the effect of wake vortex added-mass has gone unnoticed. However, as comparative biologists begin to examine the fluid dynamics of animal swimming and flying more closely, instantaneous forces and wake vortex added-mass can no longer be overlooked. The present paper supports the development of methods to estimate these locomotive dynamics from wake measurements, by presenting models that are compatible with current experimental capabilities. A primary challenge that has not been fully resolved here is the quantitative determination of wake vortex boundaries. This information is needed to determine the shape and size of the wake vortices, from which the wake vortex added-mass coefficient can be empirically determined. In the present case, the frame transformation method of Dabiri and Gharib (2004) has been implemented. This method will likely be effective for studying radially symmetric vortex ring wakes such as those generated by jellyfish (cf. Fig. 9; Dabiri et al., 2005), squids and salps; however, it cannot be used to elucidate the structure of more complex wakes.

In general, a Lagrangian particle tracking method (such as that of S. C. Shadden, J. O. Dabiri and J. E. Marsden, manuscript submitted for publication) will be needed, since the Eulerian velocity field has been shown to be ineffective in determine the vortex boundary. Alternatively, the vortex boundary can be roughly estimated based on the spatial distribution of the wake vorticity.

Fig. 9. DPIV measurements of a free-swimming *Aurelia aurita* jellyfish. Images are taken in the laser sheet plane, which is aligned close to the plane of symmetry of the animal. Vortex wake of the free-swimming jellyfish consists of a train of nearly axisymmetric vortex rings (white arrows; cores numbered in order of formation). Flow field is approximately 14 cm in height.

In this paper, we have primarily concerned ourselves with linear vortex acceleration corresponding to the diagonal elements of the added-mass tensor. It is prudent to note the possibility that the angular acceleration components of the added-mass tensor may also contribute to swimming and flying dynamics in some special cases. Further work is needed to develop methods to quantify these components and to infer their contribution to the dynamics of animal swimming and flying. It is expected that the dynamics of turning and rotating maneuvers will depend heavily on these additional added-mass effects.

Finally, it is important to note that vortex formation is not the only time during the stroke cycle when large vortex accelerations may lead to a measurable force contribution from wake vortex added-mass. Any time the animal body and/or appendages interact with vortices in the flow, the resulting vortex acceleration or deceleration can result in substantial added-mass forces. The author hypothesizes that these interactions are integral to the observed effectiveness of wake capture (e.g. Dickinson et al., 1999) and other body–vortex interactions (e.g. Liao et al., 2003) that characterize animal swimming and flying. Recent results suggest that these interactions can be optimized by animals (Dabiri and Gharib, 2005).

List of symbols

A	wake vortex loop area
C	Bernoulli variable
$\mathbf{C}_{AM}$	added-mass tensor
c_{ii}	added-mass coefficient
$\overline{c_{ii}}$	two-dimensional added-mass coefficient
d_0	initial body-plane separation distance
dS	control surface element
$\hat{f}$	characteristic frequency
$\mathbf{F}$	locomotive force
$\mathbf{F}_T$	total force
$\overline{F_V}$	time-averaged vertical fluid dynamic force
$\mathbf{F}_V$	vertical fluid dynamic force
$\mathbf{i}$, $\mathbf{j}$, $\mathbf{k}$	Cartesian unit vectors
$\hat{l}$	characteristic length scale
l	generic length unit
L/D	jet length-to-diameter ratio
mg	animal body weight
$\mathbf{n}$	unit normal vector
p	fluid pressure
r_L	Lagrangian particle plane radius
s	generic time unit
S	wake vortex width
$\hat{St}$	generic Strouhal number
St	locomotion Strouhal number
S_V	surface of vorticity-containing region
T	propulsive stroke duration
t	time
$\mathbf{U}$	body translational velocity
$\hat{U}$	characteristic velocity
$\mathbf{u}$	Eulerian velocity field
u, v, w	Cartesian velocity components
$\mathbf{U}_{Vi}$	wake vortex velocity in i-direction
V	control volume
$V(t)$	vertical flight speed
V_V	volume of vorticity-containing region
Wa	wake vortex ratio
$\mathbf{x}(t)$	Lagrangian particle trajectory
x, y, z	Cartesian coordinate directions
$Y(t)$	vertical flight trajectory
Ω_B	body volume
Ω_D	drift volume
Ω_V	wake vortex volume
$\Omega_{D,partial}$	partial drift volume
$d\Omega_E/dt$	ambient fluid entrainment rate
$d\Omega_V/dt$	wake vortex volume growth rate
ϵ_Γ	circulation measurement uncertainty
ϕ	velocity potential
ρ	fluid density
ρ_B	body density
ρ_M	medium density
Γ	wake vortex circulation
$\boldsymbol{\omega}$	vorticity field

The author gratefully acknowledges the comments of the anonymous reviewers of this manuscript, as well as discussions with M. H. Dickinson, A. Leonard, D. I. Pullin, P. S. Krueger and M. Gharib.

References

Batchelor, G. K. (1967). *An Introduction to Fluid Dynamics*. Cambridge: Cambridge University Press.

Benjamin, T. B. (1986). Note on added mass and drift. *J. Fluid Mech.* **169**, 251-256.

Bush, J. W. M. and Eames, I. (1998a). Fluid displacement by high Reynolds number bubble motion in a thin gap. *Int. J. Multiphas. Flow* **24**, 411-430.

Dabiri, J. O. and Gharib, M. (2004). Fluid entrainment by isolated vortex rings. *J. Fluid Mech.* **511**, 311-331.

Dabiri, J. O. and Gharib, M. (2005). The role of optimal vortex formation in biological fluid transport. *Proc. R. Soc. Lond. B* **272**, 1557-1560.

Dabiri, J. O., Colin, S. P., Costello, J. H. and Gharib, M. (2005). Vortex motion in the ocean: *in situ* visualization of jellyfish swimming and feeding flows. *Phys. Fluids* (in press).

Daniel, T. L. (1983). Mechanics and energetics of medusan jet propulsion. *Can. J. Zool.* **61**, 1406-1420.

Daniel, T. L. (1984). Unsteady aspects of aquatic locomotion. *Am. Zool.* **24**, 121-134.

Darwin, C. (1953). Note on hydrodynamics. *Proc. Cam. Phil. Soc.* **49**, 342-354.

Dickinson, M. H., Lehmann, F. O. and Sane, S. P. (1999).Wing rotation and the aerodynamic basis of insect flight. *Science* **284**, 1954-1960.

Drucker, E. G. and Lauder, G. V. (1999). Locomotor forces on a swimming fish: Three-dimensional vortex wake dynamics quantified using digital particle image velocimetry. *J. Exp. Biol.* **202**, 2393-2412.

Eames, I. (2003). The concept of drift and its application to multiphase and multibody problems. *Phil. Trans. A* **361**, 2951-2965.

Eames, I. and Duursma, G. (1997). Displacement of horizontal layers by bubbles injected into fluidized beds. *Chem. Eng. Sci.* **52**, 2697-2705.

Eames, I. and Flor, J.-B. (1998). Fluid transport by dipolar vortices. *Dynam. Atmos. Oceans* **28**, 93-105.

Eames, I., Belcher, S. E. and Hunt, J. C. R. (1994). Drift, partial drift and Darwin's proposition. *J. Fluid Mech.* **275**, 201-223.

Krueger, P. S. and Gharib, M. (2003). The significance of vortex ring formation to the impulse and thrust of a starting jet. *Phys. Fluids* **15**, 1271-1281.

Liao, J. C., Beal, D. N., Lauder, G. V. and Triantafyllou, M. S. (2003). Fish exploiting vortices decrease muscle activity. *Science* **302**, 1566-1569.

Milne-Thompson, L. M. (1968). *Theoretical Hydrodynamics*. New York: Dover Publications.

Noca, F., Shiels, D. and Jeon, D. (1997). Measuring instantaneous fluid dynamic forces on bodies, using only velocity fields and their derivatives. *J. Fluid Struct.* **11**, 345-350.

Noca, F., Shiels, D. and Jeon, D. (1999). A comparison of methods for evaluating time-dependent fluid dynamic forces on bodies, using only velocity fields and their derivatives. *J. Fluid Struct.* **13**, 551-578.

Saffman, P. G. (1992). *Vortex Dynamics*. Cambridge: Cambridge University Press.

Smits, A. J. (2000). *A Physical Introduction to Fluid Mechanics*. New York: John Wiley and Sons.

Spedding, G. R., Rosen, M. and Hedenstrom, A. (2003). A family of vortex wakes generated by a thrush nightingale in free flight in a wind tunnel over its entire natural range of flight speeds. *J. Exp. Biol.* **206**, 2313-2344.

Sunada, S. and Ellington, C. P. (2001). A new method for explaining the generation of aerodynamic forces in flapping flight. *Math. Method Appl. Sci.* **24**, 1377-1386.

Taylor, G. K., Nudds, R. L. and Thomas, A. L. R. (2003). Flying and swimming animals cruise at a Strouhal number tuned for high power efficiency. *Nature* **425**, 707-711.

Usherwood, J. R., Hendrick, T. L., McGowan, C. P. and Biewener, A. A. (2005). Dynamic pressure maps for wings and tails of pigeons in slow, flapping flight, and their energetic implications. *J. Exp. Biol.* **208**, 355-369.

Warrick, D. R., Tobalske, B. W. and Powers, D. R. (2005). Aerodynamics of the hovering hummingbird. *Nature* **435**, 1094-1097.

Weihs, D. (1977). Periodic jet propulsion of aquatic creatures. *Forts. Zool.* **24**, 171-175.